Title

OH-Initiated Heterogeneous Oxidation of Internally-Mixed Squalane and Secondary Organic Aerosol

Journal

Environmental Science & Technology, 48(6)

ISSN

0013-936X 1520-5851

Authors

Kolesar, Katheryn R
Buffaloe, Gina
Wilson, Kevin R
et al.

Publication Date

2014-03-18

DOI

10.1021/es405177d

Peer reviewed

Title: **OH-initiated Heterogeneous Oxidation of Internally-Mixed Squalane and Secondary Organic Aerosol**

Authors:

Katheryn R. Kolesar[1], Gina Buffaloe[1], Kevin R.Wilson[2] and Christopher D. Cappa[1,*]

Author affiliation:

[1]Department of Civil and Environmental Engineering, University of California, Davis, One Shields Avenue, Davis, California 95616

[2]Chemical Sciences Division, Lawrence Berkeley National Laboratory, One Cyclotron Rd, Berkeley, California 94720 United States

Corresponding author:

Christopher D. Cappa[1,*] - One Shields Ave, Department of Civil and Environmental Engineering, University of California Davis, Davis, CA 95616, phone: (530) 752-8180, e-mail: cdcappa@ucdavis.edu

Keywords: heterogeneous oxidation, secondary organic aerosol, aerosol

Abstract

Recent work has established that secondary organic aerosol (SOA) can exist as an amorphous solid, leading to various suggestions that the addition of SOA coatings to existing particles will decrease the reactivity of those particles towards common atmospheric oxidants. Experimental evidence suggests that O_3 is unable to physically diffuse through an exterior semi-solid or solid layer thus inhibiting reaction with the core. The extent to which this suppression in reactivity occurs for OH has not been established, nor has this been demonstrated specifically for SOA. Here, measurements of the influence of adding a coating of α-pinene+O_3 SOA onto squalane particles on the OH-initiated heterogeneous oxidation rate are reported. The chemical composition of the oxidized internally-mixed particles was monitored on-line using a vacuum ultraviolet-aerosol mass spectrometer. Variations in the squalane oxidation rate with particle composition were quantified by measurement of the effective uptake coefficient, γ_{eff}, which is the loss rate of a species relative to the oxidant-particle collision rate. Instead of decreasing, the measured γ_{eff} increased continuously as the SOA coating thickness increased, by a factor of ~2 for a SOA coating thickness of 42 nm (corresponding to ca. two thirds of the particle mass). These results indicate that heterogeneous oxidation of ambient aerosol by OH radicals is not inhibited by SOA coatings, and further that condensed phase chemical pathways and rates in organic particles depend importantly on composition.

34 **Graphical Abstract**

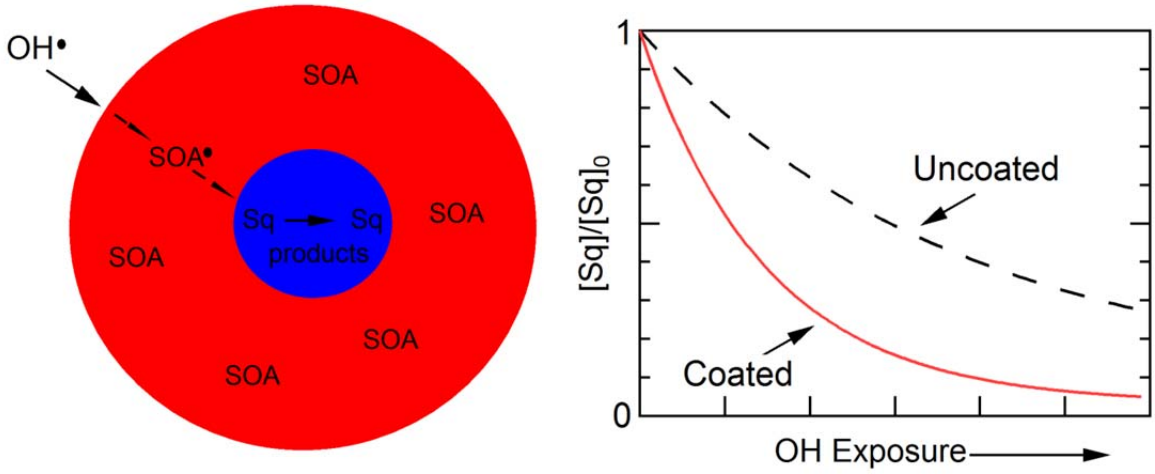

35

Introduction

Atmospheric particulate matter (PM) affects human health,[1] visibility and climate.[2] PM is comprised of both organic and inorganic compounds, with the organic fraction comprising 20-90% of the submicron particle mass.[3] The organic aerosol (OA) fraction is a complex mixture of hundreds of different species of both primary (directly emitted; POA) and secondary (gas-to-particle conversion; SOA) origin. SOA is often the dominant fraction of OA.[4] In addition to the production of condensable species from gas-phase reactions and subsequent formation of SOA, both condensed phase and heterogeneous (gas + particle) reactions can modify the chemical composition and physical properties of ambient OA on varying timescales. Heterogeneous oxidation reactions typically alter particle hygroscopicity[5, 6] and can cause particle mass loss,[7] thereby affecting particle lifetime[8] and both direct and indirect radiative effects. Further, heterogeneous oxidation complicates the use of the individual POA molecules as quantitative "tracers" for source apportionment.[9-11] Previous studies using various model POA types (e.g. squalane,[12] dioctyl sebacate,[13] pyrene[8] or motor oil[14]) indicate that heterogeneous oxidation by OH radicals is efficient, with observed reactive uptake coefficients (i.e. the probability that an OH-molecule collision results in loss of particle phase species) greater than 0.1.

The complexity of heterogeneous reactions within atmospheric OA is not fully captured in the study of single component model aerosols,[14-18] with most multiple-component studies to date focused on ozone-initiated reactions and with few that consider the influence of SOA condensation on POA oxidation.[19] Since SOA and POA will co-exist within the same individual particles in the atmosphere it is important to characterize how SOA condensation onto POA influences particle reactivity. The influence of SOA on heterogeneous reactivity of particles is of particular interest as recent studies have shown that SOA can be an amorphous solid with very high viscosity, rather than a liquid mixture,[20] leading to various suggestions that heterogeneous oxidation rates might be substantially slowed when particles obtain an SOA coating.[21-25] Indeed, there is experimental evidence that the reactivity of organic compounds within particles towards O_3 can be reduced after coating by[26] or mixing with[27-29] a solid, non-reactive (albeit non-SOA) species, most likely due to physical exclusion of the O_3 from the species of interest. However, it is not established whether such protection from oxidation occurs for the heterogeneous reactions of coated particles with another key atmospheric oxidant, the OH radical.

A key difference between OH and O_3 is that OH radicals react nearly universally with organic molecules while O_3 reacts predominately with species containing double bonds. Thus, direct reaction of OH radicals with the SOA coating is possible, leading to the generation of condensed phase radicals. These SOA-derived radicals could subsequently react with molecules that are buried below the particle surface, in which case the SOA would not serve as a protective coating and loss of the buried species would be entirely the result of secondary reactions in the condensed phase. Here, the influence of coating α-pinene + O_3 SOA onto squalane ($C_{30}H_{62}$), a previously well-studied[12] POA surrogate, on its heterogeneous reactivity towards OH radicals is investigated by measuring the effective reactive uptake coefficient, $\gamma_{eff,Sq}$, as a function of SOA coating thickness. The measured $\gamma_{eff,Sq}$ accounts for loss due to both direct oxidation by OH radicals and oxidation resulting from organic radical reactions occurring in the condensed phase.

Experimental

Organic Aerosol Generation

The coated aerosol was generated in two steps: (i) nucleation of the squalane seed and (ii) condensation of SOA formed by the dark ozonolysis of α-pinene onto the squalane seed particles (Fig. S1). Squalane aerosol was generated via homogeneous nucleation by passing clean, dry N_2 gas over liquid squalane heated to ~128 ^oC to produce a log-normal distribution of particles with an experiment-specific surface-area weighted median diameter, $D_{p,S}$, between 155 and 200 nm and a geometric standard deviation, σ, between 1.25 and 1.4. SOA coating was accomplished by passing the squalane seed particles through a stainless steel dark reaction tube along with variable amounts of α-pinene entrained in N_2, and variable amounts of O_3. As the α-pinene reacts with O_3 (~3 ppmv α-pinene and 9 - 14 ppmv O_3), lower volatility products are formed and condense on the squalane seed, causing the particles to grow. There is some small loss of squalane during the coating step, most likely as a result of heterogeneous reactions initiated by OH radicals generated from the O_3 + α-pinene reaction (see Supporting Information). Residual gas-phase hydrocarbons and O_3 were removed by passing the gas stream through a charcoal denuder and a denuder filled with Carulite® 200 (Carus) catalyst before entering the OH reaction flow tube. Total volume concentrations were on the order of 1000 $\mu m^3/cm^3$.

Heterogeneous Oxidation

The particles (either coated or uncoated) are oxidized by OH in the presence of O_2 in the flow tube reactor described previously in detail (Fig. S2).[7, 12] Excess O_3 from the flow tube is removed in a Carulite® denuder prior to gas or particle-phase measurements. The reacted particle size distribution was measured with an SMPS (TSI, Inc.) and the particle composition was measured using a home-built vacuum ultraviolet aerosol mass spectrometer (VUV-AMS).[30] For the experiments reported here, the aerosol was vaporized *in vacuo* at ~120 ^{o}C and photoionized using 10.5 eV radiation produced by the Chemical Dynamics Beamline (9.0.2) at the Advanced Light Source. (See Supporting Information for further details.)

Some of the flow exiting the flow tube was filtered and sampled into a gas chromatograph (GC) equipped with a flame ionization detector (SRI Instruments). The GC was used to measure the concentration of hexane in the gas stream (added as a tracer), from which the OH exposure ($\langle [OH] \rangle_t \cdot t$) in the flow tube can be determined using a mixed-phase relative rates approach.[31]

Determination of Particle Coating Thickness

The SOA coating thickness on the squalane seed particles that characterizes each experiment was determined from the difference in the median number weighted diameter, $D_{p,N}$, of the particle distribution measured before and after coating (Fig. 1). The size distribution of the uncoated particles was monitored throughout an experiment by measuring downstream of the nucleation oven but prior to the coating system. The size distribution of the coated particles was measured using a second SMPS located downstream of the reaction flow tube. The characteristic coating thicknesses ranged from 0-42 nm. The observed growth indicates that there is a distribution of coating thicknesses in a given experiment, typically with smaller particles having somewhat thinner coatings than larger particles (Fig. 1). Uncertainties in the characteristic coating thickness for a given experiment were assessed based on the observed co-variability in coated and uncoated particle size distributions. Importantly, the presence of a nucleation mode of pure SOA particles (which was occasionally observed) has no influence on the results because the decay of squalane is specifically monitored and thus observed decay rates depend only on the squalane-containing particles.

Although the observations clearly demonstrate that the SOA condensed onto the squalane particles, we do not have direct evidence that confirms the particles adopted a core-shell

morphology in which the SOA coated the squalane particles. However, results from a variety of previous studies suggest that SOA coated on squalane should adopt a core-shell morphology. SOA is compositionally much more complex than squalane, comprised of multi-functional oxygenated molecules[32] that likely form oligomers[33] with comparably greater hydrophilicity,[34] larger density ($\rho_{SOA} \sim 1.2 \mu g\ m^{-3}$)[35] and, as noted above, likely exists as an amorphous solid.[20] Such differences in composition and physical properties make it likely from a thermodynamic perspective that the SOA and squalane will not mix, and thus that the SOA forms a layer on the squalane seed particles as it condenses. Further, depth-profiling measurements of individual particles for which SOA (from α-pinene + O_3) was condensed onto dioctyl phthalate (a liquid hydrocarbon like squalane) indicate a core-shell configuration that was stable over many hours.[36] In addition, indirect observations of the condensation of α-pinene + O_3 SOA on fulvic and adipic acid core particles suggest that two phases are formed in these more hydrophilic systems as well.[37] Furthermore, when SOA particles (from the reaction of toluene + OH) were added to a chamber containing pure squalane particles, no mixing was observed on atmospherically relevant timescales, in contrast to similar experiments that used isotopically labeled liquid docosane particles, which indicates that mixing of SOA with squalane is not thermodynamically favorable.[38] Thus, the available evidence from the literature strongly suggests that the α-pinene + O_3 SOA condenses onto the squalane seed particles forming mixed particles with a core-shell morphology.

Experimental Determination of Squalane Loss Rates

The experimentally accessible parameter is the decrease in squalane relative to the unreacted particles as a function of OH exposure. The observed decay is characterized by the effective reaction rate coefficient, $k_{eff,Sq}$. The $k_{eff,Sq}$ for each experiment is measured by monitoring the loss of particle-phase squalane upon exposure of the particles to OH at steady state, as opposed to monitoring the gas-phase loss of OH. This distinction is important because the observed $k_{eff,Sq}$ (and calculated $\gamma_{eff,Sq}$) accounts both for direct reaction of OH with near-surface molecules and for any loss that occurs from secondary radical reactions within the condensed phase, which have the potential to substantially increase the rate of chemical transformations in the condensed phase, relative to the oxidant collision rate.[31, 39] The observed $k_{eff,Sq}$ therefore represent the combined effects of direct H-abstraction and secondary reactions. The measured $k_{eff,Sq}$ (cm^3

molecules^{-1} s^{-1}) is determined by fitting an exponential to the fraction of squalane remaining in the particle ($[Sq]_t/[Sq]_0$) as a function of OH exposure:

$$\frac{[Sq]_t}{[Sq]_0} = \exp^{-k_{eff,Sq}\cdot\langle[OH]\rangle_t\cdot t} \quad , \qquad (1)$$

where $[Sq]_0$ is the initial molecular density of squalane (molecules cm^{-3}), $[Sq]_t$ is the molecular density of squalane at time t, and $\langle[OH]\rangle_t \cdot t$ is determined from the measured decay of hexane (k_{Hex} = 5.2 x 10^{-12} cm^3 molecules^{-1}s^{-1})[40] in the flow tube (See *Supplemental Information*). The $[Sq]_0$ and $[Sq]_t$ for a given coating condition and OH exposure were determined from the mass spectra (Fig. 2). The parent squalane peak and several fragments that have large relative intensities exhibit little overlap with SOA in the VUV-AMS mass spectra, which allows for quantification of the squalane decay rate in the presence of SOA coatings. The observed squalane decays and the individual fits of $k_{eff,Sq}$ are shown for each coating thickness experiment in Fig. S3. Example mass spectra of unoxidized and oxidized spectra for the coated and uncoated particles are shown in Fig. S4.

Results and Discussion

Upon coating the squalane with SOA, the observed $k_{eff,Sq}$ does not decrease, even for the thickest coatings (Fig. 3 and Fig. S3). This observation provides unambiguous evidence that the condensation of SOA onto squalane does not suppress the OH-initiated oxidation of squalane. This result is particularly surprising for the particles here since they most likely have a core-shell (SOA on squalane) morphology. If the reactive uptake coefficient is > 10^{-4}, the reacto-diffusive length of OH in highly viscous (η = 10^8 Pa s)[41] SOA is << 1 nm, and even if the SOA were liquid (η = 10^{-3} Pa s) the reacto-diffusive length would be < 5 nm (Fig. S5). Therefore, once the SOA coating thickness is greater than 5 nm it will act as a physically protective coating making the frequency with which OH radicals will directly encounter a squalane molecule effectively zero, and consequently it is expected that $\gamma_{eff,Sq}$ = 0 (Fig. 4). However, a value of $\gamma_{eff,Sq}$ = 0 is inconsistent with the observation that the squalane continues to decay (i.e. $k_{eff,Sq}$ is non-zero) after addition of coatings up to 42 nm thickness.

That the squalane continues to react in the coated particles suggests that condensed phase reactions initiated from the reaction of OH radicals with the SOA coating are responsible for the

observed decay. Specifically, we hypothesize that SOA radicals formed in the condensed phase at the particle surface are able to chemically migrate through the coating, eventually encountering the molecules in the squalane core. Since squalane decay is not slowed by the addition of the SOA, this indicates that this chemical migration of radicals is rapid, despite the apparently high viscosity of the SOA coating, which suggests that this process may occur much faster than physical diffusion. Such radical migration likely occurs via a series of H-abstractions that follow from local changes in the SOA matrix upon radical formation that facilitate radical migration in highly viscous media.[42] This could involve alkyl, alkyl peroxy or alkoxy radicals. Once at the SOA-squalane interface, an SOA radical can abstract an H-atom from a squalane molecule thereby initiating the oxidation of squalane.

It is useful to consider the effective uptake coefficient for the SOA-coated squalane particles, $\gamma_{eff,Sq,coated}$, instead of $k_{eff,Sq}$ directly since $\gamma_{eff,Sq,coated}$ accounts for differences in the particle size and the frequency of OH-particle collisions between different experiments. (For example, whereas for a given system $k_{eff,Sq}$ decreases with increasing particle size, $\gamma_{eff,Sq}$ is size independent.) Values of $\gamma_{eff,Sq,coated}$ for a core-shell morphology can be determined from the observed $k_{eff,Sq}$ as:[12]

$$\gamma_{eff,Sq,coated} = \frac{4 \cdot k_{eff,Sq} \cdot \rho_{Sq} \cdot N_A}{\bar{c} \cdot MW_{Sq}} \cdot \frac{V_{uncoated}}{A_{coated}} \quad (2)$$

where ρ_{Sq} is the squalane density (ρ_{Sq} = 0.80 g cm^{-3}), N_A is Avogadro's number, $\bar{c}$ is the root mean squared speed of OH (609 m s^{-1}), MW_{Sq} is the molecular weight of squalane (422 g mol^{-1}), $V_{uncoated}$ is the volume of uncoated squalane and A_{coated} is the coated particle surface area. The $\gamma_{eff,Sq,coated}$ from Eq. 2 characterizes the observed squalane loss rate relative to the OH-particle collision rate for the entire coated particle. The $\gamma_{eff,Sq,coated}$ have not been corrected for gas-phase diffusion because the observed loss rate includes loss due to secondary, condensed phase reactions and thus depends only indirectly on the rate of OH collisions with the particle. Since this study focuses on relative changes, this is not a significant limitation.

For uncoated squalane particles, the observed average $\gamma_{eff,Sq}$ = 0.25 ± 0.05 (or 0.28 ± 0.06 after diffusion correction), consistent with previous results.[12] As the thickness of the SOA coating is increased the corresponding $\gamma_{eff,Sq,coated}$ increases, by up to a factor of ~2 for the thickest coatings,

with some indication that $\gamma_{eff,Sq,coated}$ may plateau at large coating thicknesses (Fig. 4). Thus, rather than the addition of an SOA coating causing a decrease in the loss rate of squalane, these observations demonstrate that squalane loss is actually enhanced relative to the pure squalane particles, at least over the range of coating thicknesses considered here. These results are qualitatively consistent with previous results where it was found that the coating of motor oil seed particles with SOA did not suppress the reactivity of the motor oil components towards OH, potentially with a slight increase in the bulk $\gamma_{eff,Sq,coated}$ for a thin coating.[19]

The form of Eqn. 2 and the possibility of radical propagation through the SOA coating suggests a potential for radical "focusing" towards the squalane core, which could partially explain the increase in the observed squalane loss rate. Focusing could arise because the OH reacts with the surface area of the entire particle, which is larger than the surface area of the squalane core. For the core-shell system here, the observable $\gamma_{eff,Sq,coated}$ can be broken down into the component processes and will depend on five factors:

$$\gamma_{eff,Sq,coated} = \gamma_{SOA,OH} \cdot F_{coating} \cdot p_{radical} \cdot \gamma_{Sq,SOA} \cdot L_{Sq} \quad (3)$$

where $\gamma_{SOA,OH}$ is the uptake coefficient of OH on SOA, exclusive of secondary reactions and $\gamma_{Sq,SOA}$ is the uptake coefficient of condensed-phase SOA radicals at the SOA/squalane interface, exclusive of secondary reactions within the squalane core. Secondary reactions within the squalane core that lead to squalane depletion are characterized by the radical chain propagation length, L_{Sq}; for uncoated particles $\gamma_{eff,Sq} = \gamma_{Sq,OH} \cdot L_{Sq}$, where $\gamma_{Sq,OH}$ is the uptake coefficient of OH on squalane. $F_{coating}$ characterizes the extent of geometric focusing, which depends on the ratio between the coated and uncoated particle surface areas. Finally, $p_{radical}$ is the probability that SOA radicals generated at the particle surface propagate inwards and reach the squalane-SOA interface. $p_{radical}$ is dependent on the likelihood of radical termination reactions relative to radical propagation reactions and will likely depend on the coating thickness. Given the likely high viscosity of the SOA coating, it is likely that the transport of organic radicals from the particle surface to the squalane core occurs through a process of radical transfer from molecule to molecule, i.e. chemical diffusion, rather than from physical diffusion of the radicals. In other words, the radical can 'move' inward as an outer layer radical abstracts a hydrogen atom from a molecule closer to the squalane core. There is likely to be a balance between the competing

dependencies of $F_{coating}$ and $p_{radical}$ on coating thickness. In general, $F_{coating}$ increases with coating thickness because the available surface area for OH+SOA reactions increases and thus the rate of radical generation in the particle is increased. The result is an increase in the number of radicals formed per squalane surface area. However, as the coating thickness increases the number of propagation reactions required for the radical to move from the surface to the squalane core increases, which will likely lead to a decrease in $p_{radical}$ with coating thickness. These competing dependencies may help to explain the observation that $\gamma_{eff,Sq}$ exhibits an approximate plateau at larger coating thicknesses. Quantitatively separating the contributions from these different terms is not possible at this point. The above conceptual model of the oxidation process in these coated particles indicates a sensitivity to radical propagation in the SOA coating, which may vary between different SOA types and should be explored in future studies.

In the above analysis it was assumed that the particles adopt a core-shell morphology, based on consideration of literature results and differences in the chemical nature of the SOA and squalane. However, at this point it is not possible to entirely rule out the possibility that the SOA and squalane are internally well-mixed, although this seems unlikely. In the well-mixed case OH radicals can react directly with squalane at the particle surface. (It is useful to note that even if the SOA and squalane are well-mixed within particles these observations indicate that condensation of SOA onto POA does not necessarily protect the POA from oxidation. Thus, even if the particles are well-mixed the loss of squalane is accelerated in the presence of SOA leading to faster oxidation in the atmosphere.) In the case of well-mixed particles the $\gamma_{eff,Sq}$ is expressed as:

$$\gamma_{eff,Sq,well-mixed} = \frac{4 \cdot k_{eff,Sq} \cdot N_A \cdot \left(\frac{VF_{Sq} \cdot \rho_{Sq}}{MW_{Sq}} + \frac{VF_{SOA} \cdot \rho_{SOA}}{MW_{SOA}} \right)}{\bar{c}} \cdot \frac{D_{p,S,coated}}{6} \quad (4)$$

where $D_{p,S}$ is the surface area weighted median diameter of the coated particle distribution, MW_{SOA} is the assumed mean molecular weight of SOA molecules, ρ_{SOA} is the SOA density (~ 1.2 g cm^{-3}), and VF_{Sq} and VF_{SOA} are the volume fractions of squalane and SOA, respectively, in the unoxidized particles (see Supporting Information). The average MW of SOA is not particularly well established. Monomer products of α-pinene + O_3 have MWs of ~200 amu, but there is some evidence that α-pinene + O_3 SOA is comprised of a substantial fraction of dimers

and trimers, which would increase the average MW.[43] As such, $\gamma_{eff,Sq,well\text{-}mixed}$ has been calculated under the assumption that MW_{SOA} = 200 amu or 400 amu. As with $\gamma_{eff,Sq,coated}$, $\gamma_{eff,Sq,well\text{-}mixed}$ increases as coating thickness increases, but now by a much larger amount (Fig. 4). The major difference between Eq. 2 and 4, for coated versus well-mixed particles, comes about because in the well-mixed case both squalane and SOA molecules exist at the surface, and thus only a fraction of the surface area is available for direct reaction of OH radicals with squalane. (Similar arguments apply for the case in which the SOA partially coats the squalane surface, since this would decrease the exposed squalane surface area). Consequently, there are fewer OH-squalane collisions as compared to a pure squalane particle, which ends up yielding a larger $\gamma_{eff,Sq}$ relative to the core-shell morphology.

Although in both the well-mixed and core-shell cases there is an increase in the calculated $\gamma_{eff,Sq}$ with coating thickness, in the well-mixed case there would be no radical focusing and thus an alternative explanation would be required for the increase in $\gamma_{eff,Sq}$. One possibility is that chemical reactions involving squalane-derived and SOA-derived radicals differ depending on either the identities of the radical species or the stable species with which they react. It is known that condensed phase reactions can play an important role in the heterogeneous oxidation of hydrocarbons. The relative balance between direct H-abstraction by OH radicals and condensed phase radical recycling reactions has not yet been established. Nonetheless, it is reasonable to think that, in a system composed of a mixture of a multitude of oxygenated SOA molecules and squalane molecules there may be differences in rate coefficients for hydrogen abstraction from stable species by radicals in the condensed phase (whether alkyl, peroxy or alkoxy), or in branching ratios associated with radical-radical reactions. It is also possible that the more oxygenated nature of the SOA leads to greater hydrogen bonding with OH radicals at the surface and an increased surface residence time, which could potentially enhance the probability of an OH-squalane reaction.[43] This alternative explanation is offered primarily for completeness, as it is more likely that for the particular SOA + squalane system considered here the particles are not well-mixed but instead have a core-shell morphology.

Overall, these experiments reinforce the idea that the reactivity of a given particle-phase species (here, squalane) is dependent upon the matrix in which it is mixed,[14-16, 19, 27, 28, 44] and thus care must be taken when extrapolating effective uptake coefficients measured for single-component

systems to the atmosphere. Further, there are clear and important differences in how coatings influence the heterogeneous reactivity of particles towards the common atmospheric oxidants, O_3 and OH. Whereas O_3 reactivity towards particle-bound organics can be inhibited by the addition of an organic coating due to physical exclusion of O_3,[26] the fact that OH radicals can react directly with the organic coating to generate organic radicals means that the addition of an SOA coating will not generally act to protect buried species from oxidation and can even lead to an increase in oxidation rates, as demonstrated here. The lifetime of squalane with respect to OH heterogeneous reaction in pure squalane particle is ~13 days, since $\gamma_{eff,Sq} = 0.30$[12] (particle diameter = 180 nm, and 24-hour average [OH] = 10^6 molecules cm^{-3}). The experiments here indicate that the $\gamma_{eff,Sq}$ increases upon coating with SOA, by a factor of 2 for the thickest coatings. This implies a decrease in the oxidation lifetime within mixed particles to ~6-8 days, on the order of a typical particle atmospheric lifetime of 5-10 days.[3] Altogether, these results indicate that heterogeneous oxidation by OH plays an important role in transforming OA properties on atmospherically relevant time-scales, and further that the ability of an SOA coating to shield POA (or other condensed-phase species) from oxidation depends on the specific oxidant considered. Ageing and oxygenation of atmospheric organic particles can occur faster than expected based on results from single component heterogeneous oxidation studies, with consequent impacts on the atmospheric evolution of particle hygroscopicity and atmospheric lifetime. Further research should aim to establish how the chemical and physical properties of the coating, i.e. the SOA type, influence the uptake enhancement as well as aim to characterize whether there is a dependence on RH and the nature of the radical oxidant.

ASSOCIATED CONTENT

Supporting Information

Information regarding methodologies, instrumentation and derivation of equations. This material is available free of charge via the Internet at http://pubs.acs.org.

AUTHOR INFORMATION

Corresponding Author: *Phone: 530-752-8180; E-mail: cdcappa@ucdavis.edu.

Notes: The authors declare no competing financial interest.

ACKNOWLEDGEMENTS

We thank Claudia D. Chen and Anthony Kong for their assistance in data collection, Theodora Nah for experimental assistance and Christopher Ruehl and Gabriel Isaacman for useful discussions. Funding for this work was provided by the National Science Foundation (ATM-1151062), by the Atmospheric Aerosols and Health program at UC Davis. The Advanced Light Source is supported by the Director, Office of Science, Office of Basic Energy Sciences, Chemical Sciences Division of the U.S. Department of Energy under Contract No. DE-AC02-05CH1123. K. R. W. is supported by Department of Energy, Early Career Research Program, Office of Basic Energy Sciences, Chemical Sciences Division of the U.S. Department of Energy under Contract No. DE-AC02-05CH11231. This work was performed at Beamline 9.0.2 at the Advanced Light Source at Lawrence Berkeley National Laboratory.

References

1. Chen, Y. Y.; Ebenstein, A.; Greenstone, M.; Li, H. B., Evidence on the impact of sustained exposure to air pollution on life expectancy from China's Huai River policy. *Proceedings of the National Academy of Sciences of the United States of America* **2013,** *110*, (32), 12936-12941.
2. Solomon, S.; Qin, D.; Manning, M.; Alley, R.; Berntsen, T.; Bindoff, N.; Chen, Z.; Chidthaisong, A.; Gregory, J.; Hegerl, G.; Heimann, M.; Hewitson, B.; Hoskins, B.; Joos, T.; Jouzel, J.; Kattsov, V.; Lohmann, U.; Matsuno, T.; Molina, M.; Nicholls, N.; Overpeck, J.; Raga, G.; Ramaswamy, V.; Ren, J.; Rusticucci, M.; Somerville, R.; Stocker, T.; Whetton, P.; Wood, R.; Wratt, D., *IPCC Fourth Assessment Report: Climate Change 2007: The Physical Science Basis: Contribution of Working Group I to the Fourth Assessment Report of the Intergovernmental Panel on Climate Change*. Cambridge Univ Press: Cambridge, UK, 2007.
3. Kanakidou, M.; Seinfeld, J. H.; Pandis, S. N.; Barnes, I.; Dentener, F. J.; Facchini, M. C.; Van Dingenen, R.; Ervens, B.; Nenes, A.; Nielsen, C. J.; Swietlicki, E.; Putaud, J. P.; Balkanski, Y.; Fuzzi, S.; Horth, J.; Moortgat, G. K.; Winterhalter, R.; Myhre, C. E. L.; Tsigaridis, K.; Vignati, E.; Stephanou, E. G.; Wilson, J., Organic aerosol and global climate modelling: A review. *Atmospheric Chemistry and Physics* **2005,** *5*, 1053-1123.
4. Zhang, Q.; Alfarra, M. R.; Worsnop, D. R.; Allan, J. D.; Coe, H.; Canagaratna, M. R.; Jimenez, J. L., Deconvolution and quantification of hydrocarbon-like and oxygenated organic aerosols based on aerosol mass spectrometry. *Environmental Science & Technology* **2005,** *39*, (13), 4938-4952.
5. Jimenez, J. L.; Canagaratna, M. R.; Donahue, N. M.; Prevot, A. S. H.; Zhang, Q.; Kroll, J. H.; DeCarlo, P. F.; Allan, J. D.; Coe, H.; Ng, N. L.; Aiken, A. C.; Docherty, K. S.; Ulbrich, I. M.; Grieshop, A. P.; Robinson, A. L.; Duplissy, J.; Smith, J. D.; Wilson, K. R.; Lanz, V. A.; Hueglin, C.; Sun, Y. L.; Tian, J.; Laaksonen, A.; Raatikainen, T.; Rautiainen, J.; Vaattovaara, P.; Ehn, M.; Kulmala, M.; Tomlinson, J. M.; Collins, D. R.; Cubison, M. J.; Dunlea, E. J.; Huffman, J. A.; Onasch, T. B.; Alfarra, M. R.; Williams, P. I.; Bower, K.; Kondo, Y.; Schneider, J.;

Drewnick, F.; Borrmann, S.; Weimer, S.; Demerjian, K.; Salcedo, D.; Cottrell, L.; Griffin, R.; Takami, A.; Miyoshi, T.; Hatakeyama, S.; Shimono, A.; Sun, J. Y.; Zhang, Y. M.; Dzepina, K.; Kimmel, J. R.; Sueper, D.; Jayne, J. T.; Herndon, S. C.; Trimborn, A. M.; Williams, L. R.; Wood, E. C.; Middlebrook, A. M.; Kolb, C. E.; Baltensperger, U.; Worsnop, D. R., Evolution of organic aerosols in the atmosphere. *Science* **2009,** *326*, (5959), 1525-1529.

6. Cappa, C. D.; Che, D. L.; Kessler, S. H.; Kroll, J. H.; Wilson, K. R., Variations in organic aerosol optical and hygroscopic properties upon heterogeneous OH oxidation. *J. Geophys. Res.-Atmos.* **2011,** *116*.

7. Kroll, J. H.; Smith, J. D.; Che, D. L.; Kessler, S. H.; Worsnop, D. R.; Wilson, K. R., Measurement of fragmentation and functionalization pathways in the heterogeneous oxidation of oxidized organic aerosol. *Phys. Chem. Chem. Phys.* **2009,** *11*, (36), 8005-8014.

8. Molina, M. J.; Ivanov, A. V.; Trakhtenberg, S.; Molina, L. T., Atmospheric evolution of organic aerosol. *Geophysical Research Letters* **2004,** *31*, (22), 5.

9. Weitkamp, E. A.; Hartz, K. E. H.; Sage, A. M.; Donahue, N. M.; Robinson, A. L., Laboratory measurements of the heterogeneous oxidation of condensed-phase organic molecular makers for meat cooking emissions. *Environmental Science & Technology* **2008,** *42*, (14), 5177-5182.

10. Lambe, A. T.; Miracolo, M. A.; Hennigan, C. J.; Robinson, A. L.; Donahue, N. M., Effective Rate Constants and Uptake Coefficients for the Reactions of Organic Molecular Markers (n-Alkanes, Hopanes, and Steranes) in Motor Oil and Diesel Primary Organic Aerosols with Hydroxyl Radicals. *Environmental Science & Technology* **2009,** *43*, (23), 8794-8800.

11. Hennigan, C. J.; Sullivan, A. P.; Collett, J. L.; Robinson, A. L., Levoglucosan stability in biomass burning particles exposed to hydroxyl radicals. *Geophysical Research Letters* **2010,** *37*, 4.

12. Smith, J. D.; Kroll, J. H.; Cappa, C. D.; Che, D. L.; Liu, C. L.; Ahmed, M.; Leone, S. R.; Worsnop, D. R.; Wilson, K. R., The heterogeneous reaction of hydroxyl radicals with sub-micron squalane particles: A model system for understanding the oxidative aging of ambient aerosols. *Atmospheric Chemistry and Physics* **2009,** *9*, (9), 3209-3222.

13. Hearn, J. D.; Renbaum, L. H.; Wang, X.; Smith, G. D., Kinetics and products from reaction of Cl radicals with dioctyl sebacate (DOS) particles in O2: a model for radical-initiated oxidation of organic aerosols. *Physical Chemistry Chemical Physics* **2007,** *9*, (34), 4803-4813.

14. Isaacman, G.; Chan, A. W. H.; Nah, T.; Worton, D. R.; Ruehl, C. R.; Wilson, K. R.; Goldstein, A. H., Heterogeneous OH oxidation of motor oil particles causes selective depletion of branched and less cyclic hydrocarbons. *Environmental Science & Technology* **2012,** *46*, (19), 10632-10640.

15. Huff Hartz, K. E.; Weitkamp, E. A.; Sage, A. M.; Donahue, N. M.; Robinson, A. L., Laboratory measurements of the oxidation kinetics of organic aerosol mixtures using a relative rate constants approach. *J. Geophys. Res.-Atmos.* **2007,** *112*, (D4).

16. Katrib, Y.; Biskos, G.; Buseck, P. R.; Davidovits, P.; Jayne, J. T.; Mochida, M.; Wise, M. E.; Worsnop, D. R.; Martin, S. T., Ozonolysis of mixed oleic-acid/stearic-acid particles: Reaction kinetics and chemical morphology. *Journal of Physical Chemistry A* **2005,** *109*, (48), 10910-10919.

17. Katrib, Y.; Martin, S. T.; Hung, H. M.; Rudich, Y.; Zhang, H. Z.; Slowik, J. G.; Davidovits, P.; Jayne, J. T.; Worsnop, D. R., Products and mechanisms of ozone reactions with oleic acid for aerosol particles having core-shell morphologies. *J. Phys. Chem. A* **2004,** *108*, (32).

18. George, I. J.; Slowik, J.; Abbatt, J. P. D., Chemical aging of ambient organic aerosol from heterogeneous reaction with hydroxyl radicals. *Geophysical Research Letters* **2008,** *35*, (13).
19. Weitkamp, E. A.; Lambe, A. T.; Donahue, N. M.; Robinson, A. L., Laboratory measurements of the heterogeneous oxidation of condensed-phase organic molecular makers for motor vehicle exhaust. *Environmental Science & Technology* **2008,** *42*, (21), 7950-7956.
20. Kannosto, J.; Yli-Pirila, P.; Hao, L. Q.; Leskinen, J.; Jokiniemi, J.; Makela, J. M.; Joutsensaari, J.; Laaksonen, A.; Worsnop, D. R.; Keskinen, J.; Virtanen, A., Bounce characteristics of alpha-pinene-derived SOA particles with implications to physical phase. *Boreal Environment Research* **2013,** *18*, (3-4), 329-340.
21. Virtanen, A.; Joutsensaari, J.; Koop, T.; Kannosto, J.; Yli-Pirila, P.; Leskinen, J.; Makela, J. M.; Holopainen, J. K.; Poschl, U.; Kulmala, M.; Worsnop, D. R.; Laaksonen, A., An amorphous solid state of biogenic secondary organic aerosol particles. *Nature* **2010,** *467*, (7317), 824-827.
22. Koop, T.; Bookhold, J.; Shiraiwa, M.; Poschl, U., Glass transition and phase state of organic compounds: Dependency on molecular properties and implications for secondary organic aerosols in the atmosphere. *Phys. Chem. Chem. Phys.* **2011,** *13*, (43), 19238-19255.
23. Kuwata, M.; Martin, S. T., Phase of atmospheric secondary organic material affects its reactivity. *Proceedings of the National Academy of Sciences of the United States of America* **2012,** *109*, (43), 17354-17359.
24. Renbaum-Wolff, L.; Grayson, J. W.; Bateman, A. P.; Kuwata, M.; Sellier, M.; Murray, B. J.; Shilling, J. E.; Martin, S. T.; Bertram, A. K., Viscosity of alpha-pinene secondary organic material and implications for particle growth and reactivity. *Proceedings of the National Academy of Science* **2013,** *110*, (20), 8014–8019.
25. Zelenyuk, A.; Imre, D.; Beranek, J.; Abramson, E.; Wilson, J.; Shrivastava, M., Synergy between secondary organic aerosols and long-range transport of polycyclic aromatic hydrocarbons. *Environmental Science & Technology* **2012,** *46*, (22), 12459-12466.
26. Zhou, S.; Lee, A. K. Y.; McWhinney, R. D.; Abbatt, J. P. D., Burial effects of organic coatings on the heterogeneous reactivity of particle-borne benzo[a]pyrene (BaP) toward ozone. *J. Phys. Chem. A* **2012,** *116*, (26), 7050-7056.
27. Hearn, J. D.; Smith, G. D., Reactions and mass spectra of complex particles using Aerosol CIMS. *International Journal of Mass Spectrometry* **2006,** *258*, (1-3).
28. Hearn, J. D.; Smith, G. D., Measuring rates of reaction in supercooled organic particles with implications for atmospheric aerosol. *Physical Chemistry Chemical Physics* **2005,** *7*, (13), 2549-2551.
29. Knopf, D. A.; Anthony, L. M.; Bertram, A. K., Reactive uptake of O_3 by multicomponent and multiphase mixtures containing oleic acid. *J. Phys. Chem. A* **2005,** *109*, (25), 5579-5589.
30. Gloaguen, E.; Mysak, E. R.; Leone, S. R.; Ahmed, M.; Wilson, K. R., Investigating the chemical composition of mixed organic-inorganic particles by "soft" vacuum ultraviolet photoionization: The reaction of ozone with anthracene on sodium chloride particles. *International Journal of Mass Spectrometry* **2006,** *258*, (1-3), 74-85.
31. Hearn, J. D.; Smith, G. D., A mixed-phase relative rates technique for measuring aerosol reaction kinetics. *Geophysical Research Letters* **2006,** *33*, (17).
32. Yu, J. Z.; Flagan, R. C.; Seinfeld, J. H., Identification of products containing -COOH, -OH, and -C=O in atmospheric oxidation of hydrocarbons. *Environmental Science & Technology* **1998,** *32*, (16), 2357-2370.

33. Tolocka, M. P.; Jang, M.; Ginter, J. M.; Cox, F. J.; Kamens, R. M.; Johnston, M. V., Formation of oligomers in secondary organic aerosol. *Environmental Science & Technology* **2004,** *38*, (5), 1428-1434.
34. Wex, H.; Petters, M. D.; Carrico, C. M.; Hallbauer, E.; Massling, A.; McMeeking, G. R.; Poulain, L.; Wu, Z.; Kreidenweis, S. M.; Stratmann, F., Towards closing the gap between hygroscopic growth and activation for secondary organic aerosol: Part 1-Evidence from measurements. *Atmospheric Chemistry and Physics* **2009,** *9*, (12), 3987-3997.
35. Shilling, J. E.; Chen, Q.; King, S. M.; Rosenoern, T.; Kroll, J. H.; Worsnop, D. R.; DeCarlo, P. F.; Aiken, A. C.; Sueper, D.; Jimenez, J. L.; Martin, S. T., Loading-dependent elemental composition of alpha-pinene SOA particles. *Atmospheric Chemistry and Physics* **2009,** *9*, (3), 771-782.
36. Vaden, T. D.; Song, C.; Zaveri, R. A.; Imre, D.; Zelenyuk, A., Morphology of mixed primary and secondary organic particles and the adsorption of spectator organic gases during aerosol formation. *Proceedings of the National Academy of Sciences of the United States of America* **2010,** *107*, (15), 6658-6663.
37. Song, C.; Zaveri, R. A.; Shilling, J. E.; Alexander, M. L.; Newburn, M., Effect of Hydrophilic Organic Seed Aerosols on Secondary Organic Aerosol Formation from Ozonolysis of alpha-Pinene. *Environmental Science & Technology* **2011,** *45*, (17), 7323-7329.
38. Robinson, E. S.; Saleh, R.; Donahue, N. M., Organic Aerosol Mixing Observed By Single Particle Mass Spectrometry. *The Journal of Physical Chemistry A* **2013**.
39. Liu, C. L.; Smith, J. D.; Che, D. L.; Ahmed, M.; Leone, S. R.; Wilson, K. R., The direct observation of secondary radical chain chemistry in the heterogeneous reaction of chlorine atoms with submicron squalane droplets. *Phys. Chem. Chem. Phys.* **2011,** *13*, (19), 8993-9007.
40. Atkinson, R., Kinetics of the gas-phase reactions of OH radicals with alkanes and cycloalkanes. *Atmospheric Chemistry and Physics* **2003,** *3*, 2233-2307.
41. Abramson, E.; Imre, D.; Beranek, J.; Wilson, J.; Zelenyuk, A., Experimental determination of chemical diffusion within secondary organic aerosol particles. *Phys. Chem. Chem. Phys.* **2013,** *15*, (8), 2983-2991.
42. Vyazovkin, V. L.; Tolkatchev, V. A., H-atom abstraction from alcohols by alkyl radicals - cooperative effects in the reactions of alkyl radicals in glassy methanol-d_3. *Chem. Phys.* **1995,** *195*, (1-3), 313-327.
43. Slade, J. H.; Knopf, D. A., Heterogeneous OH oxidation of biomass burning organic aerosol surrogate compounds: assessment of volatilisation products and the role of OH concentration on the reactive uptake kinetics. *Phys. Chem. Chem. Phys.* **2013,** *15*, (16), 5898-5915.
44. Hearn, J. D.; Smith, G. A., Ozonolysis of mixed oleic acid/n-docosane particles: The roles of phase, morphology, and metastable states. *J. Phys. Chem. A* **2007,** *111*, (43), 11059-11065.

Figures

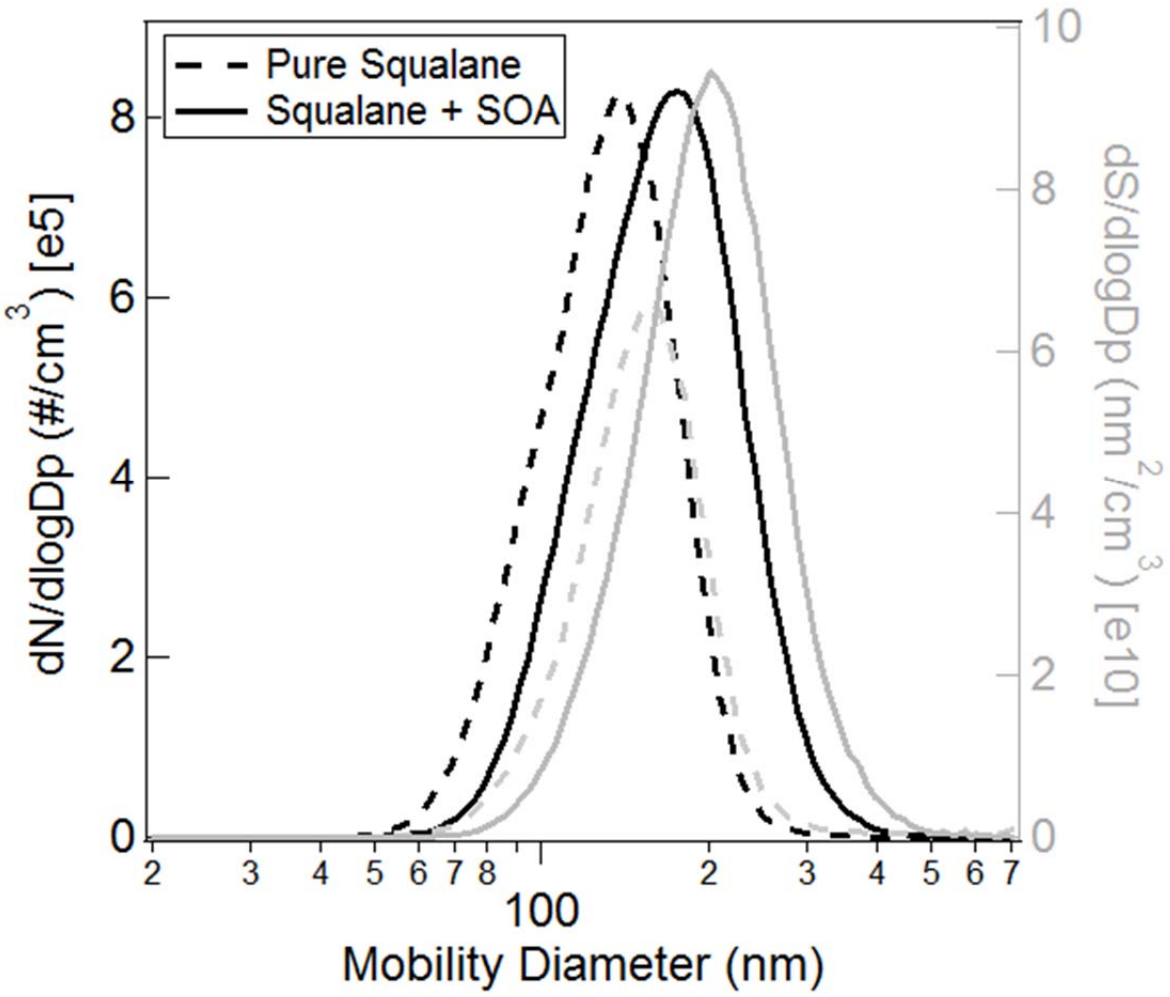

Figure 1: Example number-weighted (left axis, black lines) and surface area-weighted (right axis, gray lines) particle size distribution for uncoated (dashed line) and SOA coated (solid line) squalane particles. The initial squalane particle distribution is characterized by $D_{p,N}$ = 134 nm, σ_g = 1.30 and $N_p = 2.43*10^5$ particles cm^{-3}. After coating, the squalane particle size distribution has grown to $D_{p,N}$ = 169 nm (σ_g = 1.33, $N_p = 2.84*10^5$ particles cm^{-3}), giving a $\Delta D_{p,N}$ = 35 nm and a coating thickness of 18 nm. The average coating thickness for this experiment is 18 nm with a standard deviation of 8 nm. The slight increase in N_p upon coating for this experiment is likely indicative of fluctuations in the squalane seed particle source, and not of nucleation.

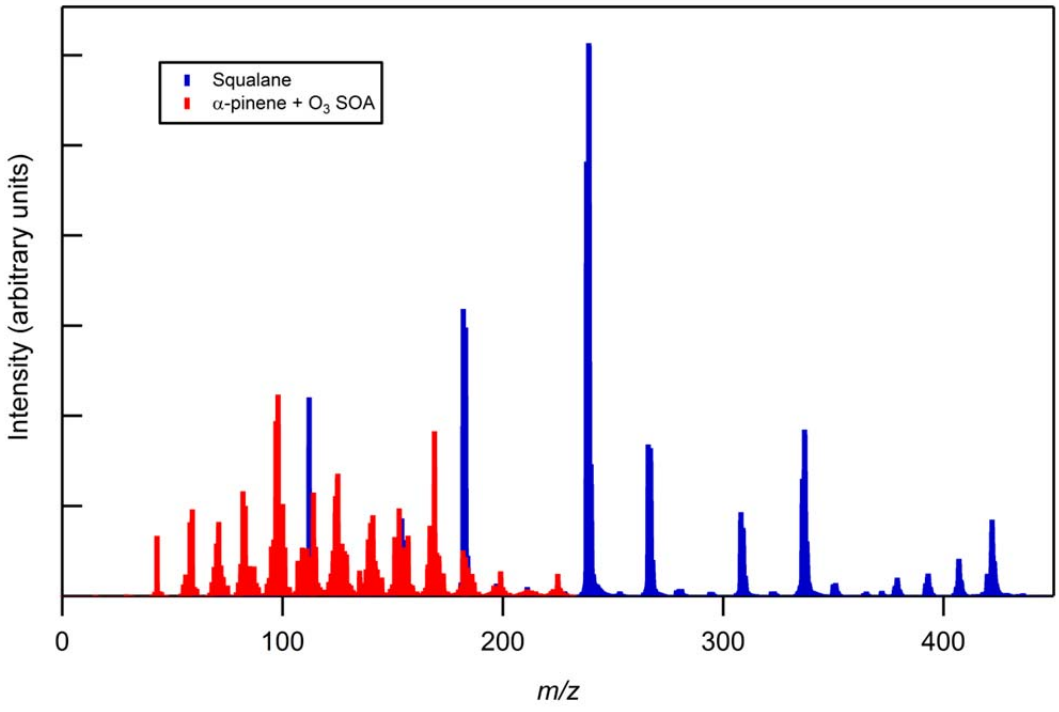

503

504 **Figure 2:** VUV-AMS spectra of pure unoxidized squalane (blue) and of unoxidized α-pinene +
505 O_3 SOA (red) as derived from a coated particle that had an average SOA coating thickness of 18
506 nm. The spectrum of the pure SOA was determined by subtracting the pure squalane signal from
507 the coated particle spectrum.

508

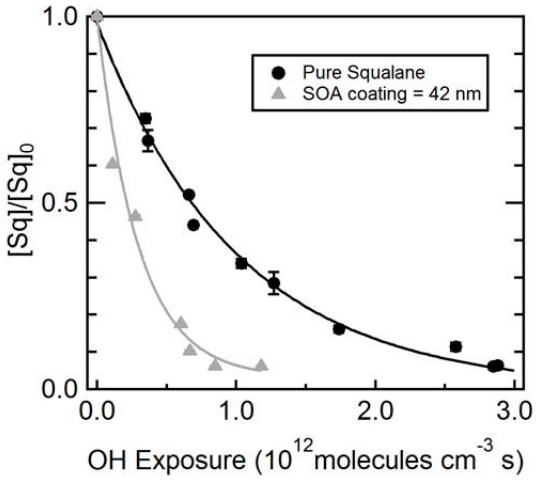

509

510 **Figure 3:** The experimentally observed squalane decay (i.e. fraction of squalane signal
511 remaining) for uncoated (black ●) and SOA-coated (grey ▲) particles. The error bars show the
512 standard deviation from the average determined from replicates of measurements made at a
513 specific OH exposure. The observed decays have been fit using a single exponential to determine
514 $k_{eff,Sq}$, where $k_{eff,Sq,uncoated} = 1.0 \times 10^{-12}$ cm^3 molecules^{-1} s^{-1} (black line) and $k_{eff,Sq,coated} = 3.5 \times 10^{-12}$
515 cm^3 molecules^{-1} s^{-1} (gray line).

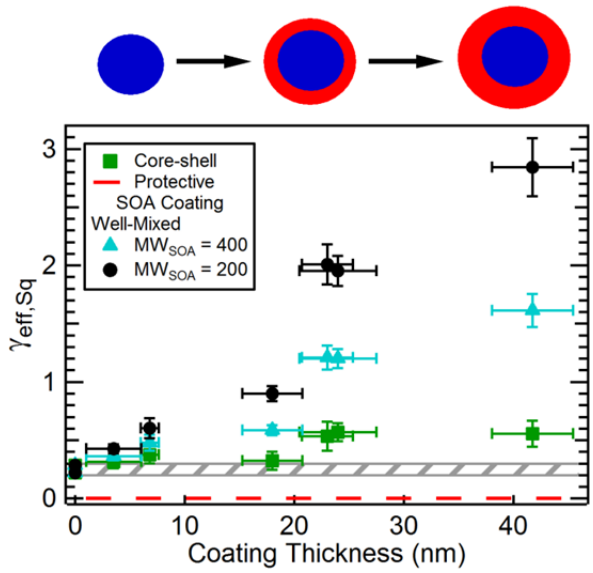

516

517 **Figure 4:** The derived $\gamma_{eff,Sq}$ as a function of SOA coating thickness under three different
518 morphology assumptions: protective SOA coating on squalane (red dashed line), core-shell
519 (green ■) and well-mixed (MW_{SOA} = 400 g/mol, blue ▲ and MW_{SOA} = 200 g/mol, black ●). The
520 cartoon above the graph illustrates the growth of the SOA coating on the squalane core for the
521 core-shell scenario. The grey hashed area indicates the value for uncoated squalane particles. The
522 uncertainty in $\gamma_{eff,Sq}$ is the greater of propagated measurement and fit uncertainties, and
523 uncertainty in the x-axis accounts for fluctuations in the coating thickness (both 1σ). For the
524 core-shell case, which is the most likely coated particle morphology, the increase in $\gamma_{eff,Sq}$ over
525 the uncoated value is a factor of ~2 at the thickest coatings considered.

Supplemental Information for "OH-initiated Heterogeneous Oxidation of Internally-Mixed Squalane and Secondary Organic Aerosol"

Katheryn R. Kolesar[1], Gina Buffaloe[1], Kevin R.Wilson[2] and Christopher D. Cappa[1,*]

[1]Department of Civil and Environmental Engineering, University of California, Davis

[2]Chemical Sciences Division, Lawrence Berkeley National Laboratory, Berkeley, California, United States

This manuscript has 14 pages and includes 5 figures.

Overview

The Supplemental Information provides details on the measurement, analysis and interpretation of VUV-AMS data. This includes discussion of (i) the experimental conditions and set-up (ii) the experimental determination of $k_{eff,Sq}$ by a mixed-phase relative rates approach (iii) the reacto-diffusive length of OH in SOA and (iv) the expanded forms of Eqn. 2 and Eqn. 4.

Organic Aerosol Generation

The coated aerosol was generated in two steps (Fig. S1). First, pure squalane aerosol was generated via homogeneous nucleation. The size distribution of the squalane seed particles was continuously monitored with a scanning mobility particle sizer (SMPS, TSI, Inc.). Second, the squalane seed was added to a dark reaction tube along with variable amounts of α-pinene entrained in N_2 (0.02 slpm), and variable amounts of O_3 (0.30 slpm, generated by passing an N_2/O_2 mixture over a pen-ray lamp). The dark ozonolysis of α-pinene generates compounds of lower volatility that condensed on the pre-existing squalane seed leading to particle growth, as monitored using a second SMPS.

Heterogeneous Oxidation

The particles (either coated or uncoated) were oxidized in a flow tube reactor by OH in the presence of O_2 (Fig. S2). The particle-laden gas stream was added to a gas-stream with 5% O_2, variable amounts of O_3, a small amount of hexane (100 ppb) that was used to determine [OH], and a mixture of dry and humidified N_2 to give a relative humidity (RH) in the flow tube of 30%. Ozone for the flow tube was generated by either (i) passing a mixture of N_2 and O_2 through a cell containing a 22.9 cm long Hg pen-ray lamp (UVP, LLC.) or (ii) using a corona discharge O_3 generator with pure O_2. Prior to adding the O_3 to the flow tube it was diluted using dry N_2. OH is produced in the flow tube from photolysis of O_3 to produce $O(^1D)$ radicals, which then react with H_2O to produce OH. The [OH] was controlled by varying the $[O_3]$ in the flow tube while keeping the RH constant at 30%. Typical O_3 concentrations in the flow tube ranged from 0-30 ppm. When the lamp was used, the amount of O_3 was varied in two ways: (i) by varying the dilution of O_3 or (ii) by varying the intensity of the lamp. When the discharge generator was used, the amount of ozone was also varied in two ways: (i) by varying the dilution of O_3 prior to addition to the flow tube or (ii) by changing the output from the generator. The O_3 concentration at the

output of the ozone generator was measured using an O_3 monitor (2B Technologies Inc.), and the concentration within the flow tube determined based on the measured [O_3] and the dilution factor. The flow tube reactor was a 130 cm long, 2.5 cm inner diameter type 219 quartz reaction cell. The flow tube was irradiated with light from four continuous output, 130 cm long Hg (λ=254 nm) lamps (UVP, LLC.). With the lights on, OH radicals were generated along the length of the flow tube from the photolysis of O_3 in the presence of water vapor. The total flow through the flow tube was 1.02 L/min, which corresponds to a residence time of 37 s along the illuminated portion of the reaction cell.

The gas stream exiting the flow tube was split between particle-phase and gas-phase measurements. Excess O_3 from the flow tube was converted to O_2 by passing the gas stream through a denuder filled with Carulite® 200 (Carus) catalyst. The reacted particle size distribution was measured with a scanning mobility particle scanner (SMPS, TSI Inc.). The particle composition was measured using a custom vacuum ultraviolet aerosol mass spectrometer (VUV-AMS). The VUV-AMS measured particle composition by sampling the particle-laden air stream through an aerodynamic lens into a high vacuum environment, impacting the resulting particle beam into a heated vaporizer where the particles are thermally vaporized, ionizing the evolved gases using VUV photoionization and detecting the resulting ions with a time-of-flight mass spectrometer.[1] For the experiments reported here, the aerosol was vaporized at ~120^{o}C and photoionized using 10.5 eV radiation produced by the Chemical Dynamics Beamline (9.0.2) at the Advanced Light Source. The VUV-AMS used here utilizes a vaporizer design that is different than in the commercial Aerodyne AMS (which has been used in some previous studies conducted at the beamline). Specifically, the vaporizer in the ALS VUV-AMS is machined out of a solid block of copper with perpendicular ports to allow passage of the VUV photon beam and impaction of the aerosol particle beam at the center of the block. There is a hole on the top of the block to allow for extraction of the ions generated from photoionization of the gas-phase molecules vaporized from the impacted particles. The bottom of the block is solid, and thus particles that "bounce" upon impaction are re-collected and can undergo evaporation and ionization. This can be contrasted with the conical collector in an Aerodyne AMS, in which particles that "bounce" are not detected. Additionally, the ALS VUV-AMS samples the particle beam and acquires spectra continuously to produce an average spectrum (here, 60 seconds) for a given condition (e.g. coating state and OH exposure).

Some of the flow was sampled into a gas chromatograph (GC) equipped with a flame ionization detector (SRI Instruments). The GC was used to measure the concentration of hexane in the gas stream, from which the average [OH] in the flow tube can be determined using a relative rates approach (see below). The sampled gas stream was passed through a filter to remove particles and a KI denuder to remove excess O_3.

The use of photoionization at 10.5 eV along with the relatively low vaporizer temperature produces mass spectra with less overall fragmentation than those observed when electron impact ionization is used with the vaporizer at 600^{o}C, as in an Aerodyne AMS. Examples of unoxidized and oxidized spectra for both coated and uncoated samples are shown in Fig. S3. The oxidized spectra are all at approximately one oxidation lifetime. As squalane becomes oxidized it is easy to see peaks that correspond to products with added ketone functionality that are spaced at 14 amu intervals from the parent squalane (*m/z* 422). Additional new peaks can be observed in the oxidized spectrum at smaller *m/z*, most likely corresponding to fragments of the squalane oxidation products produced upon vaporization/ionization, but also possibly corresponding to fragmentation oxidation products. Mass spectral peaks corresponding to SOA species are primarily in the region less than *m/z* 300 (c.f. Fig. 1 in the main text), with peaks observed at nearly every *m/z* from *m/z* 50 to *m/z* 200 and with some additional peaks at higher *m/z*. Oxidation of the coated particles leads to changes in the relative intensities of the peaks in this region, indicative of chemical changes to the SOA. Figure S3B-D also indicates that there is some small amount of oxidation of the squalane that occurs during the coating process, most likely from oxidation initiated by OH radicals formed by the ozonolysis of α-pinene.

Control Experiments

Experiments were performed where the pure squalane and SOA-coated squalane particles were exposed to O_3 within the flow tube, but with the Hg lights turned off to establish the extent to which heterogeneous reactions of O_3 with the particles or SOA production from α-pinene that was not scavenged from the air stream in the charcoal denuder occurred. No changes to either the particle size distribution nor to the measured particle mass spectrum were observed for O_3 exposure.

Experiments were performed using a similar model system, bis-2-ethylhexyl sebecate (BES) coated with α-pinene+O_3 SOA, in which the particles were passed through the flow tube with the

Hg lights on but with no O_3 to assess the extent to which direct photochemical production of radicals within the condensed phase may have influenced the current observations. Since the SOA type used is the same as in these experiments, and since no changes are observed in pure squalane particles when the Hg lights are off, the experiments using coated BES particles provide a valid test of the influence of photochemical production of condensed phase radicals. The production of BES oxidation products was not observed in the measured VUV-AMS mass spectrum for the coated particles when the particles were exposure to radiation from the Hg lamps but without O_3 present. This indicates that direct photochemical production of condensed phase radicals is not important in the current study.

Mixed-phase Relative Rates Determination of $k_{eff,Sq}$

The effective second order reaction rate constant for the reaction of squalane with OH, $k_{eff,Sq}$, was determined from an exponential fit to the observed squalane decay as a function of the OH exposure ($= \langle [OH] \rangle_t \cdot t$). The OH Exposure was determined from the measured decay of hexane in the flow tube. Since the reaction rate coefficient between hexane and OH in the gas-phase is known ($k_{Hex} = 5.2 \times 10^{-12}$ cm^3 molecules^{-1}s^{-1})[2], the OH exposure can be calculated as:

$$\frac{\ln([Hex]/[Hex]_0)}{-k_{Hex}} = \int_0^t [OH]dt = \langle [OH] \rangle_t \cdot t \qquad \text{(S1)}$$

The calculated OH exposure is then used along with the fraction of squalane remaining to determine $k_{eff,Sq}$ according to Eq. 1 in the main text. For each coating thickness experiment the observed squalane decays and the individual fits are shown in Fig. S4.

Reacto-Diffusive Length of OH in SOA

The extent to which it is possible for the OH radicals to diffusive through the SOA coating without reacting depends on the OH diffusion coefficient in the SOA matrix (D, m^{2}s^{-1}) and the first order loss rate of OH in α-pinene + O_3 SOA (k_{OH}, s^{-1}). Previous studies suggest that α-pinene + O_3 SOA is highly viscous (e.g.[3]) with $D \leq 1 \times 10^{-17}$ cm^{2}s^{-1}.[4] k_{OH} was determined from the uptake coefficient γ, which is constrained to be between 0 and 1, and the concentration of SOA molecules at the particle surface. The likelihood of an OH reaching the inner squalane core

before reacting can be characterized through consideration of the reacto-diffusive length, l_{RD}, given as:

$$l_{RD} = \sqrt{\frac{D}{k_{OH}}}. \quad \text{(S2)}$$

Values of l_{RD} have been calculated for a range of physically realistic values of D and k_{OH} (Fig. S5). As the diffusion coefficient increases (i.e. as SOA behaves more liquid-like) the l_{RD} increases. As γ, and therefore k_{OH}, increases the l_{RD} decreases. So long as the γ for SOA is > 10^{-3}, the l_{RD} of OH is less than 1 nm when $D < 10^{-7}$ cm^2 s^{-1}, i.e. even if the SOA coating has a viscosity sufficiently low to be considered "liquid-like". Consequently, for particle coating thicknesses greater than 1 nm, the OH radicals do not directly react with the squalane core.

The Effective Uptake Coefficient for a Core-Shell Morphology

In the main text the effective uptake coefficient is given as:

$$\gamma_{eff,Sq,coated} = \frac{4 \cdot k_{eff,Sq} \cdot \rho_{Sq} \cdot N_A}{\bar{c} \cdot MW_{Sq}} \cdot \frac{V_{uncoated}}{A_{coated}} \quad \text{(S1)}$$

where ρ_{Sq} is the squalane density (ρ_{Sq} = 0.80 g cm^{-3}), N_A is Avagadro's number, $\bar{c}$ is the root mean squared speed of OH (609 m s^{-1}), MW_{Sq} is the molecular weight of squalane (422 g mol^{-1}), $V_{uncoated}$ is the volume of uncoated squalane, A_{coated} is the coated particle surface area and $k_{eff,Sq}$ is the second order effective rate coefficient for loss of squalane. It was observed that the particle size distributions were reasonably log-normally distributed both for the uncoated and coated cases. Assuming log-normality, the $V_{uncoated}/A_{coated}$ term can be expanded as:

$$\frac{V_{uncoated}}{A_{coated}} = \frac{\int_0^\infty D_{uncoated}^3 f(D_{uncoated}) dD_{uncoated}}{6 \int_0^\infty D_{coated}^2 f(D_{coated})\, dD_{coated}}, \quad \text{(S2)}$$

where $D_{uncoated}$ is the uncoated particle diameter, D_{coated} is the coated particle diameter and $f(D)$is the respective normal particle distribution function:

$$f(D) = \frac{1}{\sqrt{2\pi}\cdot D\cdot ln\sigma} e^{\left(\frac{-\ln(D/\bar{D})^2}{2\cdot \ln^2 \sigma}\right)} \quad \text{(S3)}$$

Here σ is the geometric standard deviation of the log-normal distribution and $\bar{D}$ is the median diameter of the log-normal distribution.

Substituting in the distribution function, Eqn. S2 then becomes:

$$\frac{\int_0^\infty D_{uncoated}^3 f(D_{uncoated}) dD_{uncoated}}{6\int_0^\infty D_{coated}^2 f(D_{coated})\, dD_{coated}} = \frac{\frac{1}{\ln(\sigma_{uncoated})}\cdot\int_0^\infty D_{uncoated}^2 \cdot e^{-\left[\frac{\ln(D_{uncoated}/\bar{D}_{uncoated})^2}{2\cdot\ln^2\sigma_{uncoated}}\right]} dD_{uncoated}}{\frac{6}{\ln(\sigma_{coated})}\cdot\int_0^\infty D_{coated}\cdot e^{-\left[\frac{\ln(D_{coated}/\bar{D}_{coated})^2}{2\cdot\ln^2\sigma_{coated}}\right]} dD_{coated}} \quad \text{(S4)}$$

where σ_{uncoated} is the geometric standard deviation of the uncoated size distribution, σ_{coated} is the geometric standard deviation of the coated size distribution and $\bar{D}$ is median diameter of the respective (coated or uncoated) log-normal size distribution. After integration Eqn. S4 is:

$$\frac{\bar{D}_{uncoated}^2 e^{(5\ln^2\sigma_{uncoated})}}{\ln(\sigma_{uncoated})} \Big/ \frac{6\cdot\bar{D}_{coated} e^{(2\ln^2\sigma_{coated})}}{\ln(\sigma_{coated})} . \quad \text{(S5)}$$

or

$$\frac{V_{uncoated}}{A_{coated}} = \frac{\bar{D}_{uncoated}^2}{6\cdot\bar{D}_{coated}} \cdot \frac{\ln(\sigma_{coated})}{\ln(\sigma_{uncoated})} \cdot \frac{\exp(5\ln^2\sigma_{uncoated})}{\exp(2\ln^2\sigma_{coated})} \quad \text{(S6)}$$

Note that *V*/*A* for the core-shell morphology will typically be larger than *V*/*A* for the well-mixed particle type, given as Eqn. 4 in the main text. It is for this reason that the $\gamma_{\text{eff,Sq}}$ determined for the core-shell morphology is smaller than that for the well-mixed morphology for a given $k_{\text{eff,Sq}}$.

The Effective Uptake Coefficient for a Well-Mixed Morphology

For a single component system, i.e. initially pure squalane particles, the effective uptake coefficient is:

$$\gamma_{eff,Sq} = \frac{k_{eff,Sq}\cdot[Sq]\cdot[OH]}{f_{Sq}\cdot J_{coll}\cdot C_p\cdot A} \quad \text{(S7)}$$

where f_{Sq} is the fraction of squalane in the particle at a given time, J_{coll} is the OH flux at the particle surface ($\bar{c}$[OH]/4), A is the per-particle surface area and C_p is the particle number concentration. In a two component (i.e. squalane + SOA) system, the equation for the effective uptake coefficient would look similar:

$$\gamma_{eff,Sq,well-mixed} = \frac{k_{eff,Sq}\cdot[Sq]\cdot[OH]}{f_{Sq}\cdot J_{coll}\cdot C_p\cdot A} \quad \text{(S8)}$$

but now where (f_{Sq}= [Sq]/([SOA]$_0$+[Sq]$_0$)) and

$$[Sq]_0 = \frac{C_p\cdot V_{Sq}\cdot \rho_{Sq}\cdot N_A}{MW_{Sq}} \quad \text{(S9)}$$

where V_{Sq} is the per particle volume of the *uncoated* particles and N_A is Avogadro's number. However, an expression for [Sq]$_0$ can be equivalently written based on the coated particle properties, with:

$$[Sq]_0 = \frac{C_p\cdot V_{coated}\cdot VF_{Sq,0}\cdot \rho_{Sq}\cdot N_A}{MW_{Sq}} \quad \text{(S10)}$$

where V_{coated} is now the coated particle volume and $VF_{Sq,0}$ is the volume fraction of squalane in the coated particles at t = 0. Since it is a two component system, $VF_{SOA,0}$ = 1- $VF_{Sq,0}$ and

$$[SOA]_0 = \frac{C_p\cdot V_{coated}\cdot VF_{SOA,0}\cdot \rho_{SOA}\cdot N_A}{MW_{SOA}} = \frac{C_p\cdot V_{coated}\cdot (1-VF_{Sq,0})\cdot \rho_{SOA}\cdot N_A}{MW_{SOA}} \quad \text{(S11)}$$

where ρ_{SOA} is the density of SOA (~1.2 g cm^{-3} from Shilling et al.[5]) and MW_{SOA} is the molecular weight of SOA. If these definitions are substituted into the expression for f_{Sq} for the well-mixed system and into the expression for $\gamma_{eff,Sq,well-mixed}$, one obtains:

$$\gamma_{eff,Sq,well-mixed} = \frac{4 \cdot k_{eff,Sq} \cdot N_A \cdot V_{coated} \cdot \left(\frac{VF_{Sq} \cdot \rho_{Sq}}{MW_{Sq}} + \frac{VF_{SOA} \cdot \rho_{SOA}}{MW_{SOA}}\right)}{\bar{c} \cdot A_{coated}} = \frac{4 \cdot k_{eff,Sq} \cdot N_A \cdot D_{p,S,coated} \cdot \left(\frac{VF_{Sq} \cdot \rho_{Sq}}{MW_{Sq}} + \frac{VF_{SOA} \cdot \rho_{SOA}}{MW_{SOA}}\right)}{6 \cdot \bar{c}} \quad \text{(S12)}$$

which is Eq. 4 from the main text. The average MW_{SOA} is not particularly well established. Monomers of a-pinene + O_3 SOA have MWs of ~200 amu. However, there is some evidence that SOA in this system is predominately comprised of dimers and trimers[6], which would increase the average MW. Therefore $\gamma_{eff,Sq,well-mixed}$ is reported for both MW_{SOA} = 200 amu and 400 amu (Fig. 4).

References

1. Gloaguen, E.; Mysak, E. R.; Leone, S. R.; Ahmed, M.; Wilson, K. R., Investigating the chemical composition of mixed organic-inorganic particles by "soft" vacuum ultraviolet photoionization: The reaction of ozone with anthracene on sodium chloride particles. *Intl. Journ. Mass Spec.* **2006,** *258*, (1-3), 74-85.
2. Atkinson, R., Kinetics of the gas-phase reactions of OH radicals with alkanes and cycloalkanes. *Atmos. Chem. Phys.* **2003,** *3*, 2233-2307.
3. Virtanen, A.; Joutsensaari, J.; Koop, T.; Kannosto, J.; Yli-Pirila, P.; Leskinen, J.; Makela, J. M.; Holopainen, J. K.; Poschl, U.; Kulmala, M.; Worsnop, D. R.; Laaksonen, A., An amorphous solid state of biogenic secondary organic aerosol particles. *Nature* **2010,** *467*, (7317), 824-827.
4. Abramson, E.; Imre, D.; Beranek, J.; Wilson, J.; Zelenyuk, A., Experimental determination of chemical diffusion within secondary organic aerosol particles. *Phys. Chem. Chem. Phys.* **2013,** *15*, (8), 2983-2991.
5. Shilling, J. E.; Chen, Q.; King, S. M.; Rosenoern, T.; Kroll, J. H.; Worsnop, D. R.; DeCarlo, P. F.; Aiken, A. C.; Sueper, D.; Jimenez, J. L.; Martin, S. T., Loading-dependent elemental composition of alpha-pinene SOA particles. *Atmos. Chem. Phys.* **2009,** *9*, (3), 771-782.
6. Putman, A. L.; Offenberg, J. H.; Fisseha, R.; Kundu, S.; Rahn, T. A.; Mazzoleni, L. R., Ultrahigh-resolution FT-ICR mass spectrometry characterization of alpha-pinene ozonolysis SOA. **2012,** *46*, 164-172.
7. Smith, J. D.; Kroll, J. H.; Cappa, C. D.; Che, D. L.; Liu, C. L.; Ahmed, M.; Leone, S. R.; Worsnop, D. R.; Wilson, K. R., The heterogeneous reaction of hydroxyl radicals with sub-micron squalane particles: A model system for understanding the oxidative aging of ambient aerosols. *Atmos. Chem. Phys.* **2009,** *9*, (9), 3209-3222.

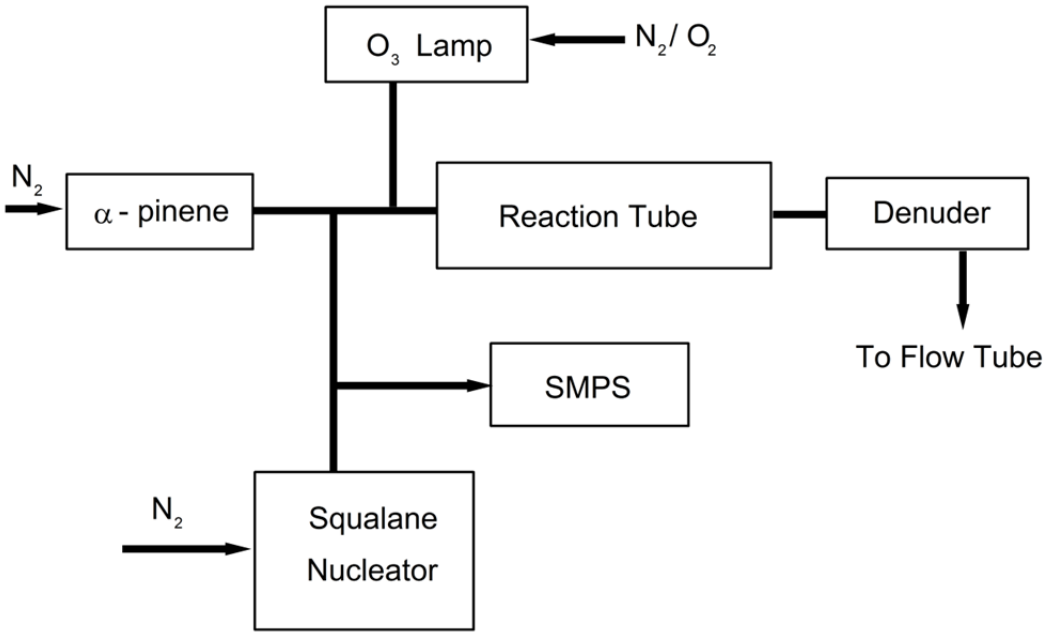

Figure S1: Schematic illustrating how the squalane particles are coated by α-pinene + O_3 SOA.

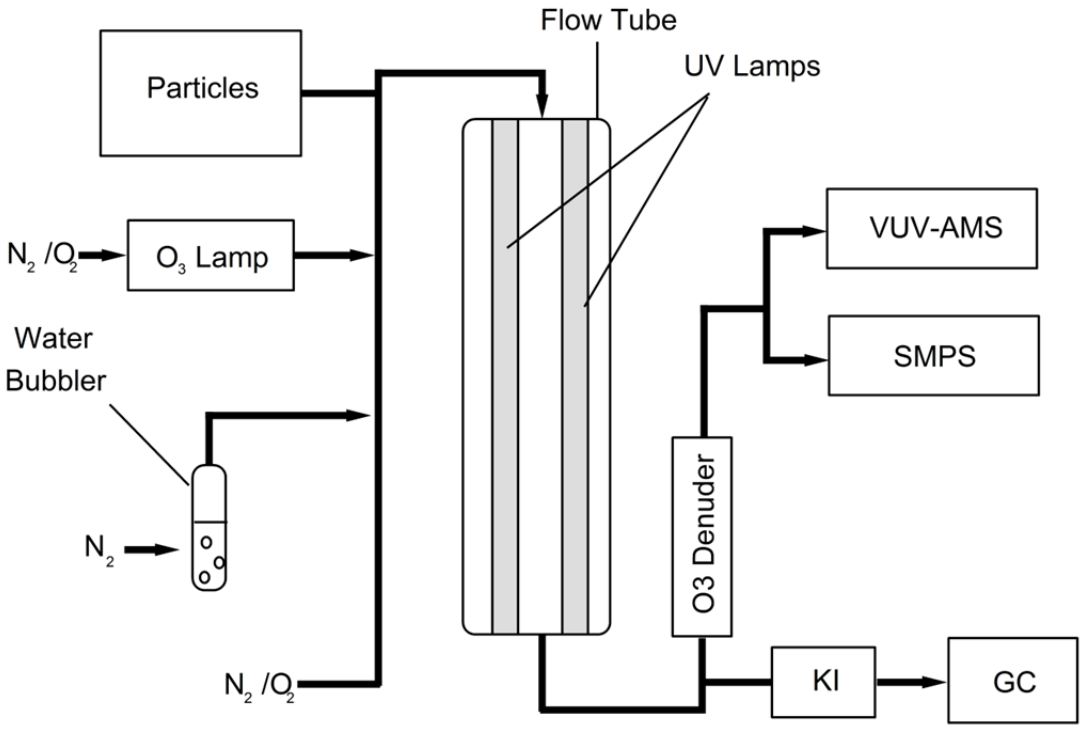

Figure S2: Schematic of experimental setup for heterogeneous oxidation of particles.

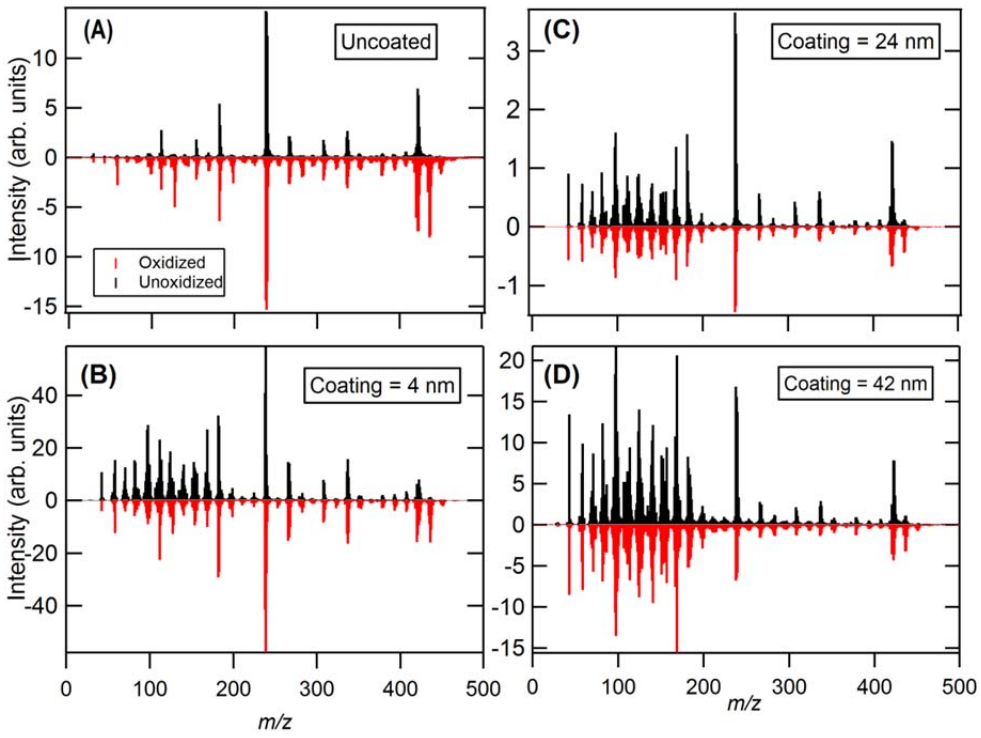

256

257 **Figure S3:** Mass spectra for unoxidized (black, positive going peaks) and oxidized (red, negative
258 going peaks) for (A) uncoated squalane and (B-D) SOA-coated squalane particles. Each oxidized
259 mass spectra is at approximately the same oxidation level, ~1 oxidation lifetime.

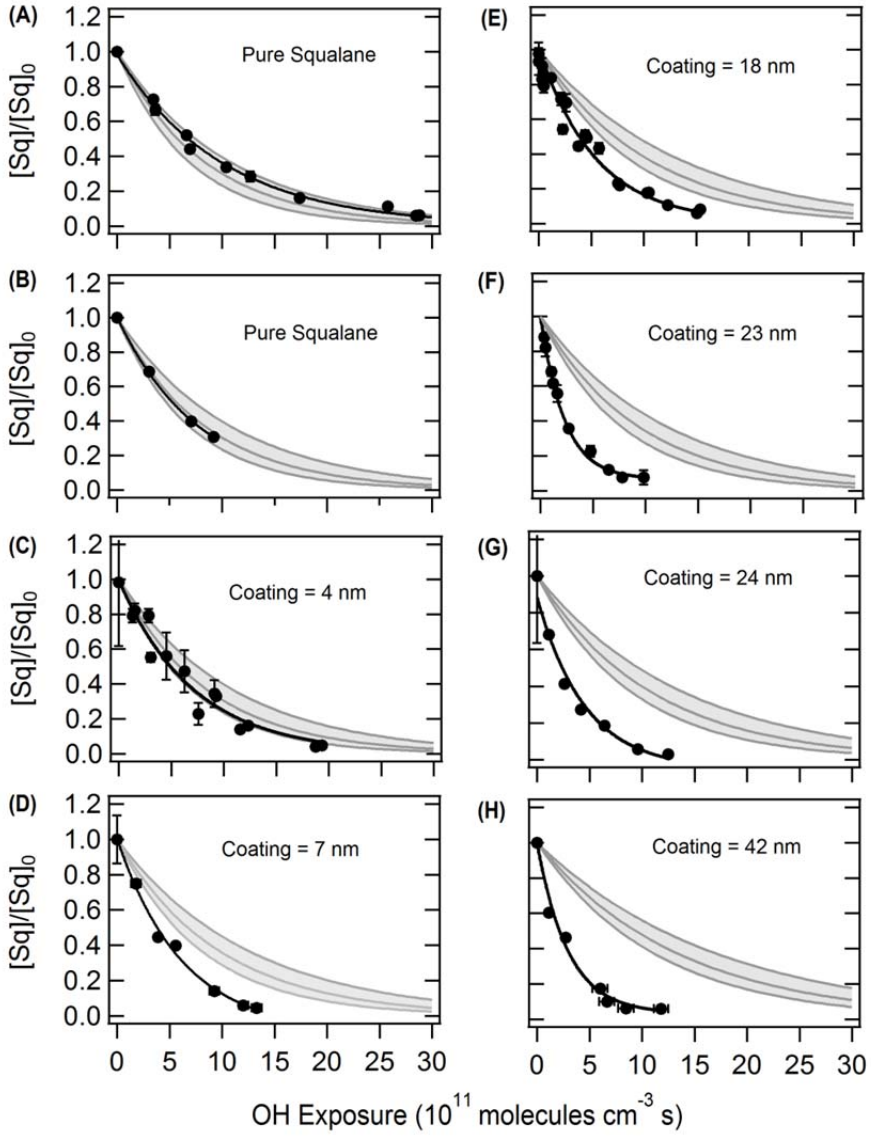

Figure S4: The observed squalane decay (i.e. fraction of squalane signal remaining) as a function of OH Exposure. Panels (A-B) shows the decay for two different uncoated squalane experiments ($D_{p,S}$ = 177 and 178 nm) and panels C-H show results for SOA coating thicknesses of (C) 4 nm (D) 7 nm (E) 18 nm (F) 23 nm (G) 24 nm and (H) 42 nm as measured using the VUV-AMS (●). The error bars show the standard deviations determined from replicates of measurements made under specific conditions. The observed decays have individually been fit to a single exponential to determine $k_{eff,Sq}$ (black lines). For reference, the grey shaded area is the predicted $k_{eff,Sq}$ based on the total surface area-weighted diameter under the assumption that $\gamma_{eff,Sq}$ = 0.30 ± 0.07 [7], which is the uncoated (diffusion corrected) value.

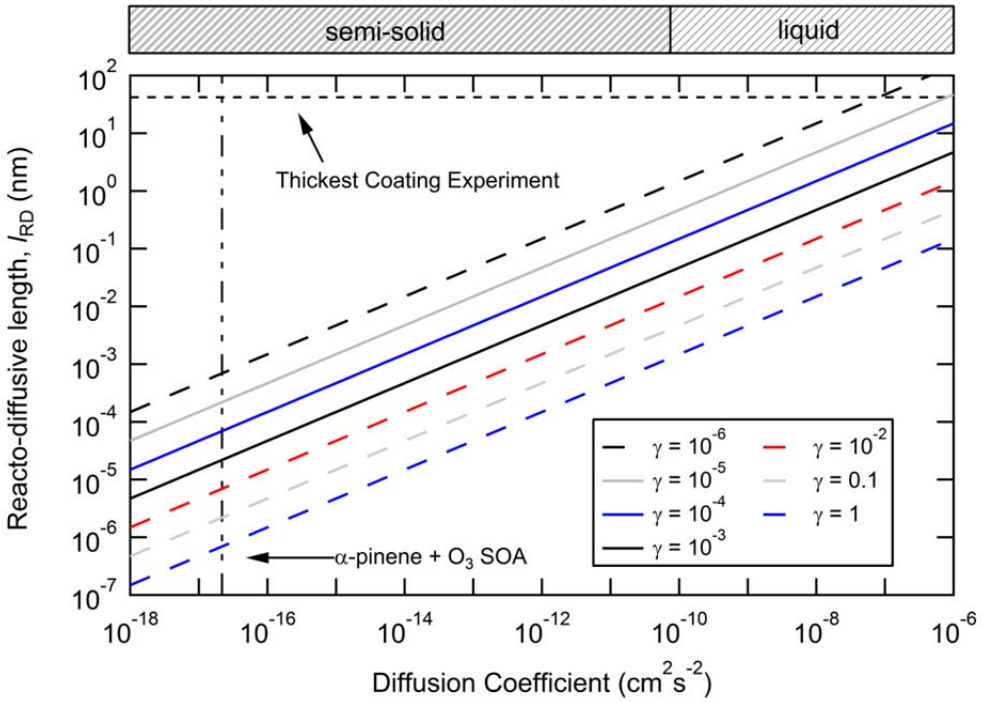

Figure S5: The reacto-diffusive length is a function of the diffusion coefficient, D, for various values of the pseudo-first order rate constant, k^1 (γ between 10^{-6} and 1). The physical phase that corresponds to a given value of D is indicated at the top of the graph.